Resonant scattering off magnetic impurities in graphene: mechanism fort ultrafast spin relaxation

D. Kochan, M. Gmitra and J. Fabian

Institute for Theoretical Physics, University of Regensburg, Regensburg, 930 40, Germany
E-mail(s): denis.kochan@ur.de, martin.gmitra@ur.de, jaroslav.fabian@ur.de
http://www.physik.uni-regensburg.de/forschung/fabian

We give a tutorial account of our recently proposed mechanism for spin relaxation based on spin-flip resonant scattering off local magnetic moments. The mechanism is rather general, working in any material with a resonant local moment, but we believe that its particular niche is graphene, whose measured spin relaxation time is 100-1000 ps. Conventional spin-orbit coupling based mechanisms (Elliott-Yafet or Dyakonov-Perel) would require large concentrations (1000 ppm) of impurities to explain this. Our mechanism needs only 1 ppm of resonant local moments, as these act as local spin hot spots: the resonant scatterers do not appear to substantially affect graphene's measured resistivity, but are dominating spin relaxation. In principle, the local moments can come from a variety of sources. Most likely would be organic molecule adsorbants or metallic adatoms. As the representative model, particularly suited for a tutorial, we consider hydrogen adatoms which are theoretically and experimentally demonstrated to yield local magnetic moments when chemisorbed on graphene. We introduce the scattering formalism and apply it to graphene, to obtain the T-matrix and spin-flip scattering rates using the generalized Fermi golden rule.

Keywords: Style file; LaTeX; Proceedings; World Scientific Publishing.

1. Introduction

Graphene[1,2] is ideal for spintronics research and applications[3,4]. The main arguments for that statement are: graphene's spin-orbit coupling is rather weak (since carbon is a light atom), the spin lifetimes of Dirac electrons in pristine graphene should be long, on the order of microseconds[5], and, as with most other properties, graphene's spin-orbit coupling and spin transport are expected to be controllable by gating, functionalization, or heterostructures building. One of those expectations, the long spin relaxation time, has not been thus far fulfilled. Spin injection experiments find, instead of microseconds, fractions of a nanosecond[6–13]. This vast discrepancy

between expectations and reality has been the most outstanding puzzle of graphene spintronics. Intense theoretical efforts have been devoted to figure out a mechanism for the ultrafast spin relaxation even in rather clean graphene sheets[14–22] to no avail. All those studies have looked at spin-orbit based spin relaxation mechanism. As was shown explicitly in Ref. 21 from first principles scattering calculations for adatom impurities on graphene, one can obtain spin relaxation times of orders of 100 ps when considering adatoms such as silicon at special positions. However, the concentration of such adatoms need to be unrealistically large, about 0.1 %.

Instead, we have considered local magnetic moments as the necessary ingredient for the ultrafast spin relaxation[23]. The key ingredient is resonant scattering. For a reasonable concentration of 1 ppm of local magnetic moments, an ordinary Born scattering would give spin lifetimes on the order of 10 ns. Resonant scattering enhances the exchange interaction between the Dirac electrons and magnetic moments, yielding spin lifetimes of 100 ps, with the electron dependence as seen in experiments. Our mechanism is supported by the experimental findings from mesoscopic transport[24], which show that the dephasing time saturates at low temperatures. This is a clear evidence of the presence of magnetic moments in experimental graphene samples. In our picture, magnetic moments formed at vacancies[25–27] and adatoms[26–28], they can act as spin hot spots[29]: they contribute little to the observed resistivity, while dominating spin relaxation.

Our mechanism is general, valid in any electronic material in which magnetic moments sit at resonant defects. However, graphene is an ideal match to this mechanism, as there is plenty of evidence of magnetic moments formed at adatoms and admolecules. To be specific, we consider here a rather crude but generic model of adatoms, parameterized by hydrogen sitting on the top position[28,30,31]. The magnetic exchange interaction is included at the adatom site only, to make the model analytically tractable. Numerical calculations for more extended exchange interactions show the same features. We use the T-matrix scattering formalism to calculate the spin relaxation time due to single (multiplied by the concentration) adatom with the local moment. What we find are the spin lifetimes of about 100 ps for as little as 1 ppm of local moments. The agreement with experiment, on the level of the electron density dependence, is reached when we average the calculated spin relaxation rates over the electron density fluctuations due to electron-hole puddles. Alternatively, the averaging can be viewed as the result of the presence of diverse adatoms with local moments, yielding a diversity of the local electronic environment. Recently, it

was found that encapsulating graphene within two-dimensional hexagonal BN, the spin relaxation time can be significantly increased [32,33]. This could be a manifestation of inhibiting magnetic impurities in such heterostructures. This direction is certainly one of the most promising to get rid of the magnetic hot spots.

This article is intended as a tutorial account of the formalism necessary to understand our mechanism. The qualitative idea is rather straightforward: in resonant scattering the electron stays a certain (called dwell) time at the defect (adatom in our case). The dwell time is the inverse of the resonance width. If the defect possesses a local magnetic moment, the electron spin will precess about that spin, with the precession period given by the inverse of the contact magnetic exchange energy. If the precession period is smaller than the dwell time, the electron spin can precess over a large angle (or even precess a few times around), so that when the electron emerges from the defect, the probability for its spin to be found in the opposite direction can be one average 50%. The criteria for the mechanism to work are i) the presence of a defect resonance peak in the density of states close (say within 100 meV) to the Dirac point, (ii) local magnetic moment at the defect, having an exchange coupling with the itinerant electrons of the magnitude greater than the width of the resonance peak. This is equivalent to saying that the spin precession period is smaller than the dwell time. Interestingly, also spin-orbit coupling can be significantly enhanced by resonant scattering. This would be the case if (iii) the spin-orbit coupling interaction energy is greater than the resonance width, in analogy with (ii). However, studies of adatoms induced spin-orbit couplings thus far exclude this possibility. It would be very interesting though to find such an adatom, since then many spin transport effects, such as spin Hall, could be greatly enhanced. Resonant scatters, magnetic or spin-orbit, lend in our view an exciting potential to graphene as a controllable spintronics material.

How the intuitive idea about resonant magnetic scattering transforms to mathematical formulas and specific numbers, is explained in this article. We show here all conceptual and calculational aspects of the scattering theory applied to graphene with adatoms and magnetic moments. Perturbative treatment ala Born approximation does not work for resonance scattering. Instead, we apply the T-matrix formalism and use the generalized Fermi golden rule to calculate the scattering rates and relaxation times. The paper is written pedagogically, with emphasis on all necessary details in order to be benefitial for students and beginners i n the field. In the first part we describe graphene essentials focusing on the tight-binding model and

Green's function techniques. In section 3 we concentrate on the momentum relaxation in the presence of non-magnetic resonant impurities. Sections 4 and 5 discuss resonant scatterers with magnetic moments like hydrogen or vacancy and the effects they have on spin relaxation.

2. Graphene essentials—tight-binding and Green's function

From the crystallographical point of view carbon atoms in graphene are arranged in a hexagonal lattice that comprises two interpenetrating triangular (Bravais) sublattices conventionally referred as A and B. The unit cell of graphene hosts two carbons—according to the sublattices they are belonging to we call them A and B—separated by the C-C distance $a_{\rm cc} = 1.42\,\text{Å}$(correspondingly, the graphene lattice constant becomes $a = \sqrt{3}a_{\rm cc} = 2.46\,\text{Å}$). The associated reciprocal lattice is also hexagonal and it possesses two nonequivalent vertices K and K′ at the Brillouin zone edges known as Dirac points. These two, as we will see, represent the Fermi momenta of a neutral system. For a visualization of the structure see the left panel of Fig. 1 and Fig. 2. The electronic band structure of graphene is illustrated at the right panel of Fig. 1. The states relevant for transport—energy window from -0.7 to 0.7 eV—form conduction and valence bands, respectively, and consist of the carbon p_z-orbitals. Their energy–momentum dispersion near the Dirac points becomes linear and consists of two touching cones whose tips meet directly at K(K′). The π-band Bloch states of graphene are formed predominantly by the carbon $2p_z$ orbitals, but the π-band symmetry allows also higher π-type atomic orbitals like $3d_{xz} \pm i3d_{yz}$. The latter are important for spin-orbit coupling[34] and will not be considered in what follows. Contrary to that the σ-bands—lying in energy from cca $-2\,\text{eV}$ below—are formed by the remaining $2s, 2p_x$ and $2p_y$ orbitals. They form sp^2 covalent hybrids, which are responsible for the robustness of graphene's structure. These essentials of the electronic band structure of graphene are known for decades, see[35–40]. We are interested in transport and relaxation processes near the Fermi level, and since there the band structure is dominated by $2p_z$ orbitals, the minimal tight-binding Hamiltonian reads

$$\mathcal{H}_{\rm gr} = -t \sum_{\langle m,n\rangle,\sigma} |m_\sigma\rangle\langle n_\sigma| + |n_\sigma\rangle\langle m_\sigma| \,. \tag{1}$$

Here the spin-resolved state $|m_\sigma\rangle$ stands for the carbon $2p_z$ electron at a lattice site m that possesses spin $\sigma \in \{1, -1\} \equiv \{\uparrow, \downarrow\}$ (quantization axis points along z-direction), the above sum over $\langle m, n\rangle$ runs over all

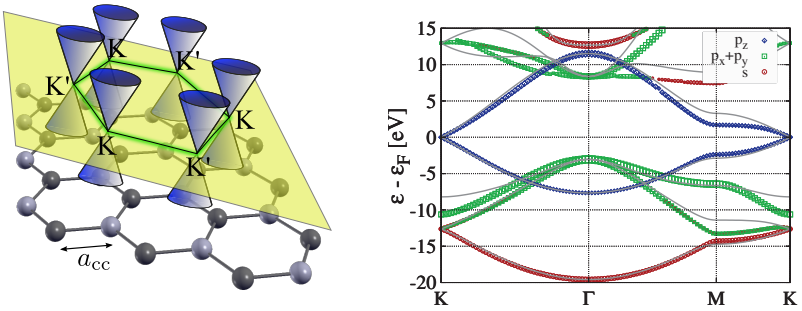

Fig. 1. Left: Graphene-essentials in cartoon—carbon atoms form a honeycomb lattice with two atoms (light and dark grey) in the unit cell. The first Brillouin zone of the reciprocal lattice (yellow plane) contains two nonequivalent Dirac points, K and K′; see also Fig. 2. The relevant conduction and valence π-bands at the Fermi level form two touching cones meeting at K(K′). The figure is adopted from Ref. 34.
Right: First-principles computation of the band structure of a graphene monolayer along the high symmetry lines in the Brillouin zone. The size of the symbols corresponds to the contribution of the given carbon atomic orbital to the Bloch eigenstate with the given momentum and the solid lines are tight-binding model solutions. The figure is adopted from Ref. 41.

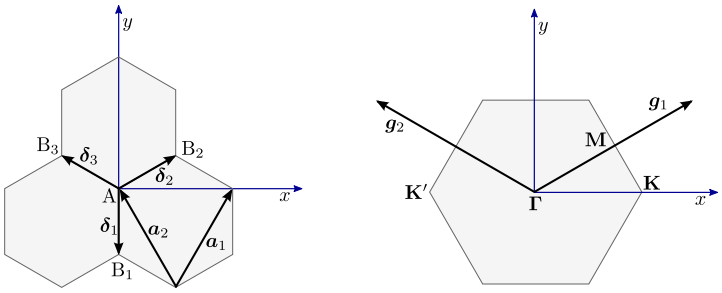

Fig. 2. Left: Graphene honeycomb lattice with the lattice vectors $\boldsymbol{a}_1$ and $\boldsymbol{a}_2$ and the nearest neighbor vectors $\boldsymbol{\delta}_\alpha$, $\alpha = 1, 2, 3$.
Right: The associated Brillouin zone with the reciprocal lattice vectors $\boldsymbol{g}_1$ and $\boldsymbol{g}_2$ and positions of the high symmetry points represented by vectors $\mathbf{\Gamma}$, $\mathbf{M}$, $\mathbf{K}$, $\mathbf{K}' = -\mathbf{K}$.

pairs of nearest-neighbors with hybridization hopping $t \simeq 2.6\,\mathrm{eV}$. When the sublattice of an atomic site m needs to be specified, we explicitly write $|m(\mathrm{A})_\sigma\rangle$ or $|m(\mathrm{B})_\sigma\rangle$. Considering a graphene sample with N unit cells and

periodic boundary conditions we can introduce Bloch states

$$\begin{aligned} |\mathbf{k}(\mathrm{A})_\sigma\rangle &= \frac{1}{\sqrt{N}} \sum_{m\in\mathrm{A}} e^{\mathrm{i}\mathbf{k}\cdot\mathbf{R}_m} |m(\mathrm{A})_\sigma\rangle \,, \\ |\mathbf{k}(\mathrm{B})_\sigma\rangle &= \frac{1}{\sqrt{N}} \sum_{m\in\mathrm{B}} e^{\mathrm{i}\mathbf{k}\cdot\mathbf{R}_m} |m(\mathrm{B})_\sigma\rangle \,, \end{aligned} \tag{2}$$

where vector $\mathbf{R}_m$ stands for the position of the m-th carbon site. Then the Hamiltonian $\mathcal{H}_{\mathrm{gr}}$ can be rewritten in the Bloch form

$$\mathcal{H}_{\mathrm{gr}} = -t \sum_{\mathbf{k},\sigma} f(\mathbf{k}) \, |\mathbf{k}(\mathrm{A})_\sigma\rangle\langle\mathbf{k}(\mathrm{B})_\sigma| + f^*(\mathbf{k}) \, |\mathbf{k}(\mathrm{B})_\sigma\rangle\langle\mathbf{k}(\mathrm{A})_\sigma| \,. \tag{3}$$

The summation over $\mathbf{k}$ runs over the 1st Brillouin zone and the structural tight-binding function $f(\mathbf{k}) = \sum_{\alpha=1}^{3} e^{\mathrm{i}\mathbf{k}\cdot\boldsymbol{\delta}_\alpha}$, where $\boldsymbol{\delta}$'s are the nearest neighbor vectors pointing from a fixed lattice site on sublattice A to its three nearest neighbors on sublattice B. The phase of $f(\mathbf{k})$ depends on the chosen orientation of the coordinate system; for our particular choice, see Fig. 2: $\boldsymbol{\delta}_\alpha = a_{\mathrm{cc}}\big(\cos[\frac{4\alpha-7}{6}\pi], \sin[\frac{4\alpha-7}{6}\pi]\big)$, where $\alpha = 1, 2, 3$.

The Bloch Hamiltonian $\mathcal{H}_{\mathrm{gr}}$ can be directly diagonalized obtaining the following eigenenergies and eigenstates:

$$\varepsilon_{\mathbf{k}\nu\sigma} = \nu t \big| f(\mathbf{k}) \big| \,, \tag{4}$$

$$|\mathbf{k}\nu\sigma\rangle = \sqrt{\frac{1}{2}} \, \big|\mathbf{k}(\mathrm{A})_\sigma\big\rangle - \nu \sqrt{\frac{f^*(\mathbf{k})}{2f(\mathbf{k})}} \, \big|\mathbf{k}(\mathrm{B})_\sigma\big\rangle \,, \tag{5}$$

where the band index ν stands for the conduction ($\nu = +1$) and valence ($\nu = -1$) band, respectively. The populated Bloch states near the Fermi level are enumerate by the crystal momenta $\mathbf{k}$ that are close to the Dirac points, i.e., $\mathbf{k} = \tau\mathbf{K} + \mathbf{q}$, where $\tau = 1$ stands for K and $\tau = -1$ for K$'$ point, respectively. In our coordinate system $\mathbf{K} = \frac{4\pi}{3a}(1, 0)$, see Fig. 2. Expanding the structural tight-binding function $f(\mathbf{k})$ around $\mathbf{K}$ we arrive at the linear dispersion relation

$$\varepsilon_{\tau\mathbf{K}+\mathbf{q}\nu\sigma} = \nu \left(\tfrac{3}{2} a_{\mathrm{cc}} t\right) |\mathbf{q}| = \nu \hbar v_F |\mathbf{q}| \,, \tag{6}$$

with the Fermi velocity $v_F = \frac{3}{2\hbar} a_{\mathrm{cc}} t \simeq 10^6 \,\mathrm{m/s}$.

The quantity we will need for later calculations is the projected retarded Green's function $G_{m_\sigma m_\sigma}(E^+) = \langle m_\sigma | (E^+ - \mathcal{H}_{\mathrm{gr}})^{-1} | m_\sigma \rangle$ for an atomic site m hosting electronic state $|m_\sigma\rangle$. The energy contains a small positive imaginary part, $E^+ = E + i\eta$. The Green's function can be obtained by direct

integration over the 1st Brillouin zone (I.B.z),

$$G_{m_\sigma m_\sigma}(E^+) = \sum_{\mathbf{k}\nu\sigma'} \frac{\langle m_\sigma|\mathbf{k}\nu\sigma'\rangle\langle\mathbf{k}\nu\sigma'|m_\sigma\rangle}{E^+ - \varepsilon_{\mathbf{k}\nu\sigma'}} \tag{7}$$

$$= \frac{1}{2N}\frac{A}{(2\pi)^2}\int\limits_{\text{I.B.z}} \mathrm{d}^2\mathbf{k}\left[\frac{1}{E^+ - t|f(\mathbf{k})|} + \frac{1}{E^+ + t|f(\mathbf{k})|}\right], \tag{8}$$

where $A/N = \frac{3}{2}\sqrt{3}a_{\text{cc}}^2$ gives the area of the graphene unit cell. The above integrals can be evaluated in terms of elliptic functions. However, in the low energy case we can compute them approximately with a very good accuracy. This will be demonstrated bellow. For the energies close to the Fermi level the most dominant contributions to the above integrals come from $\mathbf{k}$'s close to the Dirac points—Fermi momenta. Therefore, instead of the integration over the whole hexagonal Brillouin zone, we integrate only over the circles $B_2(\mathbf{K},\Lambda)$ and $B_2(-\mathbf{K},\Lambda)$ that are centered at K and K$'$ points, respectively, and which possess a cut-off radius Λ (to be specified). Moreover, we approximate $t|f(\tau\mathbf{K}+\mathbf{q})|$ by its linearized form $\hbar v_F|\mathbf{q}|$, see Eq. (6), and since the last does not depend on τ, the momentum integration over $B_2(\mathbf{K},\Lambda)\cup B_2(-\mathbf{K},\Lambda)$ is the same as twice the integration over $B_2(\mathbf{K},\Lambda)$, so in total we get

$$G_{m_\sigma m_\sigma}(E^+) \simeq \frac{2}{2N}\frac{A}{(2\pi)^2}\int\limits_{B_2(\mathbf{K},\Lambda)} \mathrm{d}^2\mathbf{q}\left[\frac{1}{E^+ - \hbar v_F|\mathbf{q}|} + \frac{1}{E^+ + \hbar v_F|\mathbf{q}|}\right]. \tag{9}$$

Introducing polar coordinates and explicitly integrating over the polar angle we arrive at

$$G_{m_\sigma m_\sigma}(E^+) = \frac{1}{N}\frac{A}{(2\pi)}\int\limits_0^\Lambda \mathrm{d}q\, q\left[\frac{1}{E^+ - \hbar v_F q} + \frac{1}{E^+ + \hbar v_F q}\right]. \tag{10}$$

The retarded Green's function we are looking for is meaningful only in the limit $\eta \to 0+$. Using the Weierstrass theorem (mind the appearance of the step functions for a finite/semi-infinite integration interval),

$$\lim_{\eta\to 0+}\int\limits_a^b \mathrm{d}x\frac{f(x)}{x - x_0 + i\eta} = \text{P.v.}\int\limits_a^b \mathrm{d}x\frac{f(x)}{x - x_0} - i\pi f(x_0)\,\Theta[x_0 - a]\Theta[b - x_0]\,,$$

we finally get

$$G_{m_\sigma m_\sigma}(E) = \frac{E}{W^2}\ln\frac{E^2}{(\hbar v_F\Lambda)^2 - E^2} - \mathrm{i}\pi\frac{|E|}{W^2}\Theta\big[\hbar v_F\Lambda - |E|\big]\,, \tag{11}$$

where $W^2 = \sqrt{3}\pi t^2$. Since $\rho(E) = -\frac{1}{\pi}\mathrm{Im}\, G_{m_\sigma m_\sigma}(E)$ is the density of states per carbon atom and spin, the momentum cut-off Λ can be specified by requiring the validity of the internal consistency condition (compare with the phonon Debye's prescription):

$$1 = \int\limits_{-\infty}^{\infty} \mathrm{d}E\, \rho(E) = \int\limits_{-\hbar v_F \Lambda}^{\hbar v_F \Lambda} \mathrm{d}E\, \frac{|E|}{W^2} = \frac{(\hbar v_F \Lambda)^2}{W^2} \quad \Rightarrow \quad \Lambda = \frac{W}{\hbar v_F} \simeq \frac{1.55}{a_{\mathrm{cc}}}\,. \quad (12)$$

Hence, we see that within the linearized theory

$$W = \sqrt{\sqrt{3}\pi t} = \hbar v_F \Lambda \simeq 6.06\,\mathrm{eV} \quad (13)$$

can be interpreted as the effective graphene bandwidth and the final form of the graphene retarded Green's function per atom and spin reads

$$G_{m_\sigma m_\sigma}(E) = \frac{E}{W^2} \ln \frac{E^2}{W^2 - E^2} - \mathrm{i}\pi \frac{|E|}{W^2} \Theta\big[W - |E|\big]\,. \quad (14)$$

Even without the direct calculation one can easily argue that $G_{m_\sigma m_\sigma}(E)$ should be spin and atomic site independent. Simply, $\mathcal{H}_{\mathrm{gr}}$, Eq. (1), does not have any spin dynamics. Hence both spin projections should behave equally. At the same time, all atomic sites are equivalent, either by lattice translation (same sublattice sites) or by translation + mirror reflection via the plane bisecting a particular C-C bond (opposite sublattice sites). To compare the effective low energy result expressed by Eq. (14) with *ab-initio* calculations we provide in Fig. 3 the density of states (DOS) per atom and spin for both cases. We see that near the Fermi level of the neutral graphene, in the energy window $[-0.5\,\mathrm{eV}, 0.5\,\mathrm{eV}]$, both DOS's match perfectly.

3. Single impurity scattering—non-perturbative approach

We focus on graphene impurity scattering assuming dilute adatom's coverage. The formulation is general and holds for any monovalent adatom that bonds covalently on the top position. However, we particulary focus on hydrogenated graphene. In the dilute coverage limit the interference effects among the wave functions outgoing from different adatom scatterers can be ignored and the problem reduces to the scattering on a single adatom (an impurity concentration enters only as a multiplicative factor).

The full Hamiltonian $\mathcal{H}$ can be separated into the graphene part $\mathcal{H}_{\mathrm{gr}}$, Eq. (1), and the chemisorption part, visualized in Fig. 4. We have,

$$\mathcal{H}_{\mathrm{orb}} = \mathcal{H}_{\mathrm{gr}} + \varepsilon \sum_\sigma |d_\sigma\rangle\langle d_\sigma| + \omega \sum_\sigma |d_\sigma\rangle\langle 0_\sigma| + |0_\sigma\rangle\langle d_\sigma|\,. \quad (15)$$

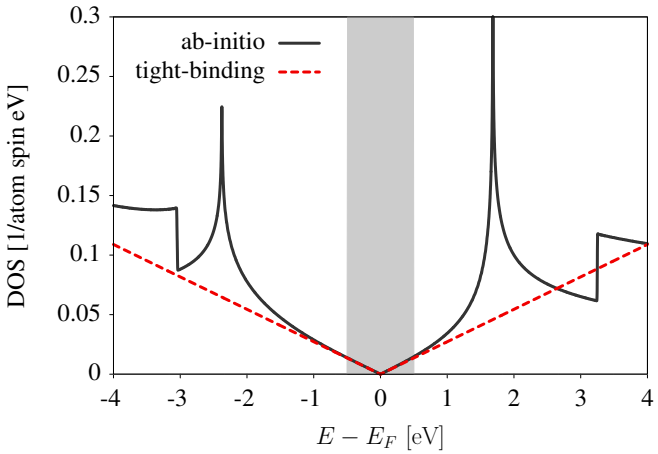

Fig. 3. Density of states per carbon atom and spin calculated from *ab-initio* (solid line) and tight-binding model (dashed line). Both DOS's match perfectly near the graphene neutrality point in the energy interval $[-0.5\,\mathrm{eV}, 0.5\,\mathrm{eV}]$ (shaded area). This would correspond to charge carriers densities varying from $[-2.5\times10^{13}\,\mathrm{cm}^{-2}, 2.5\times10^{13}\,\mathrm{cm}^{-2}]$ (the minus sign refers to holes, while the plus to electrons), well covering the experimentally accessible range.

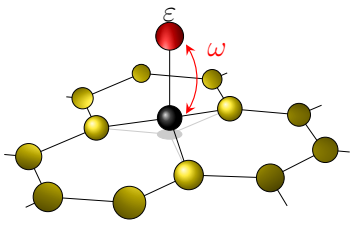

Fig. 4. Graphical representation of the chemisorption part of the tight-binding Hamiltonian $\mathcal{H}_{\mathrm{orb}}$, see Eq. (15): ε is the on-site energy of the adatom level with respect to the carbon $2p_z$ orbitals, ω is the hybridization hopping energy between the adatom orbital and the $2p_z$ orbital of the functionalized ($m = 0$) carbon site (for hydrogen [31] $\varepsilon = 0.16\,\mathrm{eV}$ and $\omega = 7.5\,\mathrm{eV}$).

Here $|d_\sigma\rangle$ is the (spin-resolved) state for the monovalent adatom level with on-site energy ε that chemisorbs via hopping ω with a carbon $2p_z$ state $|0_\sigma\rangle$ located on the atomic site $m = 0$. For hydrogenated graphene, $|d_\sigma\rangle = |1s_\sigma\rangle$. The orbital tight-binding parameters entering Eq. (15) were fitted to *ab-*

initio data in Ref. 31, $\varepsilon = 0.16\,\mathrm{eV}$ and $\omega = 7.5\,\mathrm{eV}$. For comparatione with fluorinated graphene see Ref. 42.

There is a technique how to effectively down-fold the initial Hamiltonian, Eq. (15) and eliminate the adatom $|d_\sigma\rangle$ states. We will describe the procedure with a few more details ignoring the spin. Let us look for an eigenstate $|\Psi\rangle = \psi_d|d\rangle + \sum_m \psi_m|m\rangle$ of the Hamiltonian $\mathcal{H}_{\mathrm{orb}}$ that possesses an eigenenergy E, i.e., $\mathcal{H}_{\mathrm{orb}}|\Psi\rangle = E|\Psi\rangle$. Plugging $|\Psi\rangle$ to the stationary Schrödinger equation we get a system of linear algebraic equations for the unknown amplitudes ψ_d and ψ_m:

$$E\psi_d = \varepsilon\psi_d + \omega\psi_0\,, \tag{16}$$

$$E\psi_0 = \omega\psi_d - t\sum_{\langle 0,\underline{i}\rangle}\psi_{\underline{i}}\,, \tag{17}$$

$$\vdots$$

$$E\psi_n = -t\sum_{\langle n,\underline{i}\rangle}\psi_{\underline{i}}\,, \qquad \text{for } n \neq 0\,. \tag{18}$$

Above, we have first collected all the equations that contain the amplitude ψ_d explicitly, and then we added the remaining entries that contain only graphene's carbon amplitudes. The sum over the three nearest neighbors of the given site x (0, or n in the above set of equations) is represented by the symbol $\sum_{\langle x,\underline{i}\rangle}$. Solving the first equation for the amplitude ψ_d and plugging the result $\psi_d = \frac{\omega}{E-\varepsilon}\,\psi_0$ into the second equation, we get the reduced linear system,

$$E\psi_0 = \frac{\omega^2}{E-\varepsilon}\,\psi_0 - t\sum_{\langle 0,\underline{i}\rangle}\psi_{\underline{i}}\,, \tag{19}$$

$$\vdots$$

$$E\psi_n = -t\sum_{\langle n,\underline{i}\rangle}\psi_{\underline{i}}\,, \qquad \text{for } n \neq 0\,. \tag{20}$$

The first term on the right of Eq. (19) represents an effective (energy dependent) on-site potential on the carbon site $m = 0$. Moreover, the whole reduced linear system can be equivalently generated from the Hamiltonian (for completeness the spin degrees of freedom were again restored)

$$\mathcal{H}_{\mathrm{orb}}(E) = \mathcal{H}_{\mathrm{gr}} + \frac{\omega^2}{E-\varepsilon}\sum_\sigma |0_\sigma\rangle\langle 0_\sigma|\,. \tag{21}$$

This is the down-folded effective form $\mathcal{H}_{\rm orb}(E)$ of the original Hamiltonian $\mathcal{H}_{\rm orb}$. Knowing the amplitude of eigenstate of the Hamiltonian $\mathcal{H}_{\rm orb}(E)$ on atomic site $m = 0$ that corresponds to energy $E \neq \varepsilon$, we know also the wave function amplitude on the adatom site $\psi_d = \frac{\omega}{E-\varepsilon}\,\psi_0$. For $E = \varepsilon$ we should get $\psi_0 = 0$—the carbon site $m = 0$ is effectively removed from the system—see Eq. (16), and according to Eq. (17) the amplitude $\psi_d = \frac{t}{\omega}\sum_{\langle 0,\underline{i}\rangle}\psi_{\underline{i}}$.

The scattering problem in the presence of the point-like interaction as represented by Hamiltonian $\mathcal{H}_{\rm orb}(E)$, Eq. (21), is generally solvable knowing the unperturbed Green's function $G_{0_\sigma 0_\sigma}(E) = \langle 0_\sigma|G(E)|0_\sigma\rangle$ per atom and spin for the atomic site $m = 0$. The resolvent Green's operator $\mathbb{G}$ for the full problem can be obtained by solving the corresponding Dyson equation:

$$\mathbb{G}(E^+) = G(E^+) + G(E^+)\mathrm{T}(E^+)G(E^+)\,, \tag{22}$$

$$\mathrm{T}(E^+) = \left[1 - V(E^+)G(E^+)\right]^{-1}V(E^+)\,, \tag{23}$$

where $\mathrm{T}(E^+)$ is so the called transition, or in short T-matrix, the perturbation $V(E^+) = \frac{\omega^2}{E^+-\varepsilon}\sum_\sigma |0_\sigma\rangle\langle 0_\sigma|$ is the point-like interaction entering Hamiltonian $\mathcal{H}_{\rm orb}(E^+)$ and the graphene unperturbed Green's resolvent

$$G(E^+) = \sum_{\mathbf{k}\nu\sigma} |\mathbf{k}\nu\sigma\rangle\,\frac{1}{E^+ - \varepsilon_{\mathbf{k}\nu\sigma}}\,\langle\mathbf{k}\nu\sigma|\,. \tag{24}$$

To calculate the scattering rates we need the T-matrix as a function of energy. The point-like interaction V—in the local atomic basis $\langle 0_\sigma|V(E^+)|0_\sigma\rangle = \frac{\omega^2}{E^+-\varepsilon}$ is the only non-zero element—implies that $\mathrm{T}(E^+)$ has in the atomic basis also only one non-trivial matrix element. Taking a limit $\eta \to 0+$ we get

$$\begin{aligned}\langle m_\sigma|\mathrm{T}(E)|n_{\sigma'}\rangle &= \delta_{\sigma\sigma'}\delta_{m0}\delta_{n0}\,\frac{\langle 0_\sigma|V(E)|0_\sigma\rangle}{1 - \langle 0_\sigma|V(E)|0_\sigma\rangle\,\langle 0_\sigma|G(E)|0_\sigma\rangle}\\ &= \delta_{\sigma\sigma'}\delta_{m0}\delta_{n0}\,\frac{\omega^2}{E - \varepsilon - \omega^2\,G_{0_\sigma 0_\sigma}(E)}\,,\end{aligned} \tag{25}$$

where $G_{0_\sigma 0_\sigma}(E)$ is given by Eq. (14). Even though the potential $V(E)$ is singular for $E = \omega$ the T-matrix is well defined there since $G_{0_\sigma 0_\sigma}(\omega) \neq 0$. Contrary to that, there exists in principle a finite complex energy $E_\bullet - \mathrm{i}\Gamma/2$ for which the denominator of Eq. (25) becomes zero. If this is the case the following terminology is used[43]: for $\Gamma \neq 0$ the energy $E_\bullet \equiv E_{\rm r}$ corresponds to the *scattering resonance with the lifetime* (or dwell time) $\hbar/\Gamma$, while for $\Gamma = 0$ one gets the *bound state* with the energy $E_\bullet \equiv E_{\rm b}$. Let us qualitatively explain why it is so. To have $\Gamma = 0$ the real energy $E_{\rm b}$ should be away

from the bandwidth of the unperturbed problem, i.e., $\mathrm{Im}\, G_{0_\sigma 0_\sigma}(E_\mathrm{b}) = 0$, and hence there are not available Bloch states which can scatter on that energy. On the other hand, to have $\Gamma \neq 0$ the real energy E_r should stay within the band, i.e., $\mathrm{Im}\, G_{0_\sigma 0_\sigma}(E_\mathrm{r}) \neq 0$ and hence an incident particle with the energy close to E_r will scatter very effectively as we will see in what follows. In the case of hydrogenated graphene in the low energy regime one finds

$$E_\mathrm{r} \simeq 7.4\,\mathrm{meV} \quad \text{and} \quad \Gamma \simeq 4\,\mathrm{meV}\,, \tag{26}$$

so the emerging resonance is very close to the graphene neutrality point with a lifetime (dwell time) $\tau \simeq 0.16\,\mathrm{ps}$.

The elastic scattering rate for the impurity mediated transition $|\mathbf{k}\nu\sigma\rangle \to |\mathbf{k}'\nu'\sigma'\rangle$ between two Bloch states of the unperturbed graphene is given by the Fermi golden rule and equals

$$W_{\mathbf{k}\sigma|\mathbf{k}'\sigma'} = \frac{2\pi}{\hbar}\big|\langle \mathbf{k}'\nu'\sigma' \,|\, \mathrm{T}(\varepsilon_{\mathbf{k}\nu\sigma}) \,|\, \mathbf{k}\nu\sigma\rangle\big|^2 \delta\big(\varepsilon_{\mathbf{k}\nu\sigma} - \varepsilon_{\mathbf{k}'\nu'\sigma'}\big)\,. \tag{27}$$

The energy conservation requires $\nu' = \nu$, so no interband transitions are allowed. The explicit form of the Bloch states, Eq. (5), and of the T-matrix elements, Eq. (25), enable us to write

$$W_{\mathbf{k}\sigma|\mathbf{k}'\sigma'} = \frac{2\pi}{\hbar}\frac{\delta_{\sigma\sigma'}}{(2N)^2}\left|\frac{\omega^2}{\varepsilon_{\mathbf{k}\nu\sigma} - \varepsilon - \omega^2\, G_{00}(\varepsilon_{\mathbf{k}\nu\sigma})}\right|^2 \delta\big(\varepsilon_{\mathbf{k}\nu\sigma} - \varepsilon_{\mathbf{k}'\nu'\sigma'}\big)\,, \tag{28}$$

where N is the number of graphene unit cells in the sample. In the low energy regime we would have intra- ($\tau' = \tau$) and inter- ($\tau' = -\tau$) valley transitions $\tau\mathbf{K} + \mathbf{q} \to \tau'\mathbf{K} + \mathbf{q}'$. For the Green's function $G_{00}(\varepsilon_{\mathbf{k}\nu\sigma})$ we use Eq. (14) and instead of $\varepsilon_{\mathbf{k}\nu\sigma}$ we substitute its linearized form given by Eq. (6). So the transition rate $W_{\tau\mathbf{K}+\mathbf{q}\sigma|\tau'\mathbf{K}+\mathbf{q}'\sigma'}$ can be evaluated in a closed form. Here we explicitly see again that for the incoming energy $\varepsilon_{\mathbf{k}\nu\sigma}$ that is close to the system resonance E_r, the denominator in Eq. (28) gets minimal and we have an enhanced transition rate, i.e., strong momentum scattering.

Summing the transition rates $W_{\mathbf{k}\sigma|\mathbf{k}'\sigma'}$, Eq. (28), over all the final states we get the inverse lifetime $1/\tau_{\mathbf{k}\sigma}(E)$ of a one-electron state $|\mathbf{k}\nu\sigma\rangle$ with the energy $E \equiv \varepsilon_{\mathbf{k}\nu\sigma}$. Since the whole $\mathbf{k}'$ dependence is in the delta-function, the summation over the final states gives DOS for the given spin projection σ, i.e. $2N \times |E|/W^2$ (the number of carbons times DOS per atom and spin) and we arrive at

$$\frac{1}{\tau_{\mathbf{k}\sigma}(E)} \equiv \frac{1}{\tau_\mathrm{m}(E)} = \frac{2\pi}{\hbar}\,\eta_\mathrm{imp}\left|\frac{\omega^2}{E - \varepsilon - \frac{\omega^2}{W^2}\big[E \ln\frac{E^2}{W^2} - i\pi\,|E|\big]}\right|^2 \frac{|E|}{W^2}\,. \tag{29}$$

In the above formula, the energy E is assumed to lie near the neutrality point, i.e., $|E| \lesssim 0.5\,\mathrm{eV} \ll W$, and $\eta_{\mathrm{imp}} = \frac{1}{2N}$ is the impurity concentration per carbon atom. Moreover, since $1/\tau_{\mathbf{k}\sigma}$ does not depend on $\mathbf{k}$ it is also with the average escape rate $1/\tau_{\mathrm{life}}(E)$ and the momentum relaxation rate $1/\tau_{\mathrm{m}}(E)$ at the energy E. The left panel in Fig. 5 shows the momentum-relaxation rate as a function of energy (lower scale) and also charge carriers areal density (upper scale). We see that near the resonant energy $E_{\mathrm{r}} \simeq 7.4\,\mathrm{meV}$ the momentum relaxation strongly enhances as expected from the above discussion.

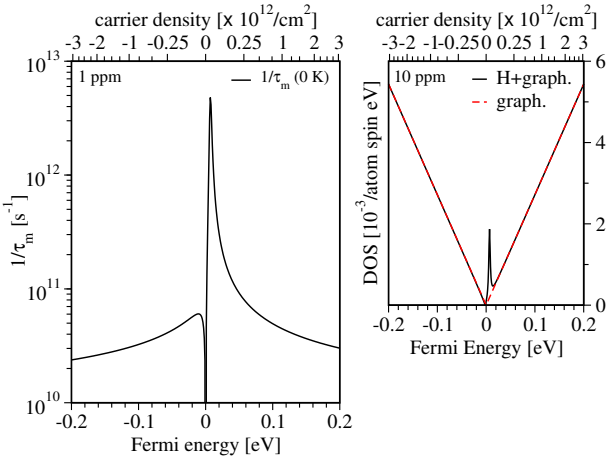

Fig. 5. Left: Momentum relaxation $1/\tau_{\mathrm{m}}$ at zero temperature as a function of the Fermi level (lower scale) and charge carriers density (upper scale) for the impurity concentration $\eta_{\mathrm{imp}} = 1\,\mathrm{ppm}$. Relaxation increases near the resonance energy—for hydrogenated graphene $E_{\mathrm{r}} \simeq 7.4\,\mathrm{meV}$. Right: Density of states per carbon and spin for hydrogenated graphene (solid line) and unperturbed graphene (dashed line). To amplify the resolution we used impurity concentration $\eta_{\mathrm{imp}} = 10\,\mathrm{ppm}$.

For completeness let us analyze the density of states $\mathcal{V}(E)$ in the presence of impurity scatterers. For that we need to compute $-\frac{1}{\pi}\,\mathrm{Im}\,\mathrm{Tr}\,\mathbb{G}(E)$, where the perturbed Green's resolvent $\mathbb{G}(E)$ is given by the Dyson Eq. (22). The unperturbed graphene DOS $-\frac{1}{\pi}\,\mathrm{Im}\,\mathrm{Tr}\,G(E)$ is known and equals $4N \times \frac{|E|}{W^2}\Theta[W - |E|]$. The trace of the interaction term $G(E)\mathrm{T}(E)G(E)$ can be recast as

$$\mathrm{Tr}\,[G(E)\mathrm{T}(E)G(E)] = \mathrm{Tr}\,[G^2(E)\mathrm{T}(E)] = \mathrm{Tr}\,[-\tfrac{dG(E)}{dE}\mathrm{T}(E)]\,. \qquad (30)$$

Computing the last expression in the local atomic basis we arrive at the formula whose entries are known explicitly,

$$\begin{aligned}\mathrm{Tr}\,[\tfrac{dG(E)}{dE}\mathrm{T}(E)] &= \\ &= \sum_{m\sigma}\langle m_\sigma|\tfrac{dG(E)}{dE}\mathrm{T}(E)|m_\sigma\rangle = \sum_{\sigma}\langle 0_\sigma|\tfrac{dG(E)}{dE}|0_\sigma\rangle\,\langle 0_\sigma|\mathrm{T}(E)|0_\sigma\rangle \qquad (31)\\ &= \sum_{\sigma}\big[\tfrac{d}{dE}\langle 0_\sigma|G(E)|0_\sigma\rangle\big]\,\mathrm{T}_{0_\sigma 0_\sigma}(E) = \sum_{\sigma}\big[\tfrac{d}{dE}G_{0_\sigma 0_\sigma}(E)\big]\,\mathrm{T}_{0_\sigma 0_\sigma}(E)\,.\end{aligned}$$

The above calculation is simple because the T-matrix has a very simple form in the local atomic basis, see Eq. (25). So the sought for perturbed DOS becomes

$$\mathcal{V}(E) = 4N\,\frac{|E|}{W^2}\Theta\big[W-|E|\big] - \frac{1}{\pi}\,\mathrm{Im}\sum_{\sigma}\big[-\tfrac{d}{dE}G_{00}(E)\big]\,\mathrm{T}_{0_\sigma 0_\sigma}(E)\,. \qquad (32)$$

The right panel in Fig. 5 compares $\frac{1}{4N}\mathcal{V}(E)$ (solid line) with the unperturbed graphene DOS per atom and spin (dashed line). We observe clearly the formation of the narrow resonance peak at energy $E_\mathrm{r} \simeq 7.4\,\mathrm{meV}$.

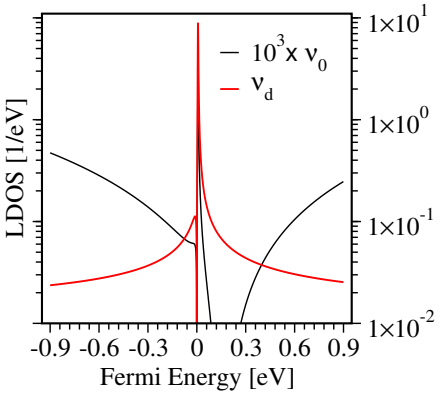

Fig. 6. Local density of states $\nu_0(E)$ and $\nu_d(E)$ on functionalized carbon (red thick line) and impurity site (black thin line), respectively, as functions of Fermi level. For a better resolution the LDOS on functionalized carbon was magnified by a factor 10^3. At the resonant energy, the impurity LDOS amplifies, describing the localization of the resonant state near the impurity.

Let us conclude this section with a few more words about resonant scattering. Looking for the scattering solution $|\Psi\rangle = \psi_d|d\rangle + \sum_m \psi_m|m\rangle$ of the Schrödinger equation for an energy near the resonance energy E_r, one finds

that $|\psi_m|^2$ becomes "localized" around the impurity site[44]. Asymptotically $|\psi_m|^2$ falls off with increasing distance from the impurity according to a power law. In Fig. 6 we plot the local DOS's ν_0 and ν_d for the functionalized carbon and the impurity site, respectively,

$$\nu_0(E) = -\frac{1}{\pi}\,\mathrm{Im}\langle 0|\mathbb{G}(E)|0\rangle = \frac{|E|}{W^2} - \frac{1}{\pi}\,\mathrm{Im}\,\frac{\left[\omega\, G_{00}(E)\right]^2}{E-\varepsilon-\omega^2\, G_{00}(E)}\,, \tag{33}$$

$$\nu_d(E) = \frac{\omega^2}{E-\varepsilon}\,\nu_0(E)\,, \tag{34}$$

confirming the above scenario. Why are we seeing a momentum relaxation enhancement near the resonances? To build a "power law localized" scattering state in the position space one would need a superposition of many Bloch states $|\Psi\rangle = \sum_{\mathbf{k}} c(\mathbf{k})|\mathbf{k}\rangle$ where $c(\mathbf{k})$ would be a widely "delocalized" function in $\mathbf{k}$-space. Hence the scattering at the resonant energy would very effectively mix $\mathbf{k}$-vectors among different $|\mathbf{k}\rangle$-states and we should expect a pronounced enhancement of the momentum relaxation as already seen in Fig. 5. A cartoon-like visualization of the resonant and off-resonant scattering on a short-range impurity is shown in Fig. 7.

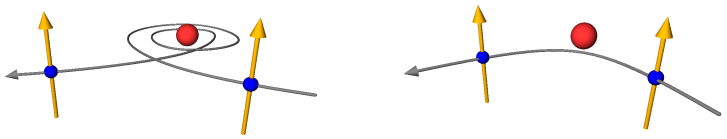

Fig. 7. Resonant scattering (left): an incoming particle $|\mathbf{k}\rangle$ with an energy close to the system resonance becomes effectively "trapped" by the impurity and "spends" a time $\hbar/\Gamma$ within the impurity region, before decaying to an extended outgoing state $|\mathbf{k}'\rangle$ with a completely randomized momentum orientation. Off-resonant scattering (right): particle scatters on the short-range impurity potential "immediately" and its momentum changes more "gradually".

4. Impurity scattering with exchange interaction

We investigate now resonant scattering in the presence of a magnetic exchange interaction. This would lead to a nontrivial spin dynamics near the system orbital resonances and would offer a new spin relaxation mechanism[23] with a potential to explain the short relaxation times in graphene.

Our previously studied Hamiltonian $\mathcal{H}_{\rm orb}$, Eq. (15), is now extended by including the exchange coupling that is located at the impurity site, i.e.,

$$\begin{aligned}\mathcal{H} &= \mathcal{H}_{\rm gr} + \varepsilon \sum_\sigma |d_\sigma\rangle\langle d_\sigma| + \omega \sum_\sigma |d_\sigma\rangle\langle 0_\sigma| + |0_\sigma\rangle\langle d_\sigma| - J\,\hat{\mathbf{s}}_d \cdot \hat{\mathbf{S}} \\ &= \mathcal{H}_{\rm orb} - J\,\hat{\mathbf{s}}_d \cdot \hat{\mathbf{S}}\,. \end{aligned} \tag{35}$$

We assume that the adatom hosts a local magnetic moment with spin $\frac{1}{2}$— described by the vector operator $\hat{\mathbf{S}}$:

$$\hat{\mathbf{S}}^x = |\Uparrow\rangle\langle\Downarrow| + |\Downarrow\rangle\langle\Uparrow|\,,\quad \hat{\mathbf{S}}^y = \tfrac{1}{\mathrm{i}}|\Uparrow\rangle\langle\Downarrow| - \tfrac{1}{\mathrm{i}}|\Downarrow\rangle\langle\Uparrow|\,,\quad \hat{\mathbf{S}}^z = |\Uparrow\rangle\langle\Uparrow| - |\Downarrow\rangle\langle\Downarrow|\,,$$

that interacts with the itinerant electron spin when this hops into the adatom $|d\rangle$-level. Analogously, $\hat{\mathbf{s}}_d$ stands for the vector of spin operators for $|d\rangle$-state (in our definition without conventional $\frac{\hbar}{2}$ factor)

$$\hat{\mathbf{s}}_d^x = |d_\uparrow\rangle\langle d_\downarrow| + |d_\downarrow\rangle\langle d_\uparrow|\,,\quad \hat{\mathbf{s}}_d^y = \tfrac{1}{\mathrm{i}}|d_\uparrow\rangle\langle d_\downarrow| - \tfrac{1}{\mathrm{i}}|d_\downarrow\rangle\langle d_\uparrow|\,,\quad \hat{\mathbf{s}}_d^z = |d_\uparrow\rangle\langle d_\uparrow| - |d_\downarrow\rangle\langle d_\downarrow|$$

and J is a constant with the dimension of energy. For the exchange we take $J = -0.4\,\mathrm{eV}$ since this value is consistent with a more detailed parametrization of the magnetic impurity model as discussed in Ref. 23. In fact the precise value of J is not important as long as $J \gg \Gamma$. First, the spin relaxation is broadened by puddles[45], and second, in graphene also other adatoms or vacancies give magnetic moments[46]. Eventually, one would need to average over the ranges of adatom hoppings with different exchange parameters (we lump this averaging under puddle broadening). Moreover, we do not discuss here the origin and a more complex microscopic model which would lead to the exchange Hamiltonian, Eq. (35), in a certain limit. Neither we do assume that J could be quenched or modified when changing the Fermi level of graphene.

In the independent electron-impurity picture (we do not discuss Kondo physics), the natural one-electron basis reads $|m_{\sigma,\Sigma}\rangle$, where the additional spinor index Σ describes the non-itinerant (local) magnetic moment $|\Sigma\rangle$. In the model Hamiltonian, Eq. (35), the term $\mathcal{H}_{\rm orb}$ acts trivially on the local spinors as well as the itinerant ones (up and down dynamics are decoupled), so it is convenient to write

$$\mathcal{H}_{\rm orb} = \big[\mathcal{H}_{\rm gr} + \varepsilon|d\rangle\langle d| + \omega|d\rangle\langle 0| + \omega|0\rangle\langle d|\big] \otimes \mathrm{Id}_\sigma \otimes \mathrm{Id}_\Sigma\,. \tag{36}$$

For practical reasons we keep the shortened form, understanding that $\mathcal{H}_{\rm orb}$ acts in the above specified sense. The full Hamiltonian $\mathcal{H}$, Eq. (35), can be easily diagonalized introducing the singlet ($\ell = 0$) and triplet ($\ell = 1$)

spinor basis $|\ell,\mu_\ell\rangle$ (here μ_ℓ runs from $-\ell$ to ℓ) combining electron spin $|\sigma\rangle$ and the adatom magnetic moment $|\Sigma\rangle$. Specifically,

$$|0,0\rangle = \tfrac{1}{\sqrt{2}}\big\{|\uparrow\rangle|\Downarrow\rangle - |\downarrow\rangle|\Uparrow\rangle\big\}\,, \qquad \begin{aligned} |1,+\rangle &= |\uparrow\rangle|\Uparrow\rangle\,,\\ |1,0\rangle &= \tfrac{1}{\sqrt{2}}\big\{|\uparrow\rangle|\Downarrow\rangle + |\downarrow\rangle|\Uparrow\rangle\big\}\,,\\ |1,-\rangle &= |\downarrow\rangle|\Downarrow\rangle\,, \end{aligned} \tag{37}$$

so our new one-electron basis now reads $|m_{\ell,\mu_\ell}\rangle = |m\rangle\otimes|\ell,\mu_\ell\rangle$. The above transformation is unitary in the composed spin space so $\mathcal{H}_{\rm orb}$ remains unchanged. The exchange term gives

$$-J\,\hat{\mathbf{s}}_d\cdot\hat{\mathbf{S}} = -J\sum_{\ell}\sum_{\mu_\ell}(4\ell-3)|d_{\ell,\mu_\ell}\rangle\langle d_{\ell,\mu_\ell}|\,. \tag{38}$$

So in total we get four decoupled Hamiltonians, $\mathcal{H}=\sum_{\ell,\mu_\ell}\mathcal{H}_{\ell,\mu_\ell}$—each singlet-triplet spin component ℓ,μ_ℓ evolves independently—namely

$$\begin{aligned}\mathcal{H} = &\sum_{\ell,\mu_\ell}\mathcal{H}_{\rm gr}(\ell,\mu_\ell) + \\ &+\big[\varepsilon - J(4\ell-3)\big]|d_{\ell,\mu_\ell}\rangle\langle d_{\ell,\mu_\ell}| + \omega\Big\{|d_{\ell,\mu_\ell}\rangle\langle 0_{\ell,\mu_\ell}| + |0_{\ell,\mu_\ell}\rangle\langle d_{\ell,\mu_\ell}|\Big\}\,,\end{aligned} \tag{39}$$

where $\mathcal{H}_{\rm gr}(\ell,\mu_\ell) = -t\sum_{\langle m,n\rangle}|m_{\ell,\mu_\ell}\rangle\langle n_{\ell,\mu_\ell}| + \text{h.c.}$ is the nearest neighbor graphene Hamiltonian for the fixed ℓ,μ_ℓ.

Now our story starts to repeat and we can quickly profit from the results discussed in the previous section. First, eliminating by down-folding the $|d_{\ell,\mu_\ell}\rangle$-orbital for each ℓ,μ_ℓ component, we get an effective down-folded Hamiltonian $\mathcal{H}(E)$ [compare with Eq. (21)],

$$\mathcal{H}(E) = \sum_{\ell,\mu_\ell}\mathcal{H}_{\rm gr}(\ell,\mu_\ell) + \alpha_\ell(E)\,|0_{\ell,\mu_\ell}\rangle\langle 0_{\ell,\mu_\ell}|\,. \tag{40}$$

The energy-dependent on-site coupling $\alpha_\ell(E)$, given by

$$\alpha_\ell(E) = \frac{\omega^2}{E-\varepsilon+(4\ell-3)J}\,, \tag{41}$$

becomes different for the singlet and triplet sectors of $\mathcal{H}(E)$. Second, it is straightforward to write down the matrix elements of the T-matrix, namely

$$\langle m_{\ell,\mu_\ell}|\mathrm{T}(E)|n_{\ell',\tilde{\mu}_{\ell'}}\rangle = \frac{\delta_{\ell\ell'}\,\delta_{\mu\tilde{\mu}}\,\delta_{m0}\,\delta_{n0}}{1/\alpha_\ell(E)-G_{00}(E)} \equiv \delta_{\ell\ell'}\,\delta_{\mu\tilde{\mu}}\,\delta_{m0}\,\delta_{n0}\,\mathrm{T}_\ell(E) \tag{42}$$

where $G_{00}(E)$ is the unperturbed Green's function per atom and spin, see Eq. (14) and

$$\mathrm{T}_\ell(E) = \frac{1}{1/\alpha_\ell(E)-G_{00}(E)} = \frac{\omega^2}{E-\varepsilon+(4\ell-3)J-\omega^2 G_{00}(E)}\,. \tag{43}$$

So the T-matrix as the operator has a very simple expression in the local atomic basis,

$$\mathrm{T}(E) = \sum_{\ell,\mu_\ell} \mathrm{T}_\ell(E)\, |0_{\ell,\mu_\ell}\rangle\langle 0_{\ell,\mu_\ell}| \,. \tag{44}$$

We wish to calculate the relaxation rates for scattering processes $|\mathbf{k}\nu\sigma\rangle \to |\mathbf{k}'\nu'\sigma'\rangle$ between the Bloch states of the unperturbed graphene that possess various spin-polarizations. For that we need to compute $\langle \mathbf{k}'\nu'\sigma' \,|\, \mathrm{T}(E=\varepsilon_{\mathbf{k}\nu\sigma}) \,|\, \mathbf{k}\nu\sigma\rangle$. Specifically,

$$\langle \mathbf{k}'\nu'\uparrow |\mathrm{T}(E)|\mathbf{k}\nu\uparrow\rangle = \frac{1}{2N}\mathrm{T}_1(E)\,|\Uparrow\rangle\langle\Uparrow| + \frac{1}{2N}\frac{\mathrm{T}_1(E)+\mathrm{T}_0(E)}{2}\,|\Downarrow\rangle\langle\Downarrow|\,, \tag{45}$$

$$\langle \mathbf{k}'\nu'\downarrow |\mathrm{T}(E)|\mathbf{k}\nu\uparrow\rangle = \frac{1}{2N}\frac{\mathrm{T}_1(E)-\mathrm{T}_0(E)}{2}\,|\Uparrow\rangle\langle\Downarrow|\,, \tag{46}$$

where the factors $\frac{1}{2N}$ come from the projections of the Bloch states, Eq. (5), onto the $m=0$ carbon site which hosts impurity. Factor $\frac{\mathrm{T}_1(E)\pm\mathrm{T}_0(E)}{2}$ comes from the decomposition of the singlet-triplet states to the original spin basis. To get the scalar quantity $\left|\langle \mathbf{k}'\nu'\sigma' \,|\, \mathrm{T}(E) \,|\, \mathbf{k}\nu\sigma\rangle\right|^2$ which enters the Fermi golden rule we should get rid off the spin degree of freedom of the local magnetic moment. This is done by

$$\begin{aligned}\left|\langle \mathbf{k}'\nu'\sigma' \,|\, \mathrm{T}(E) \,|\, \mathbf{k}\nu\sigma\rangle\right|^2 = \\ = \mathrm{Tr}_\Sigma\Big[\langle \mathbf{k}'\nu'\sigma' \,|\, \mathrm{T}(E) \,|\, \mathbf{k}\nu\sigma\rangle^\dagger \langle \mathbf{k}'\nu'\sigma' \,|\, \mathrm{T}(E) \,|\, \mathbf{k}\nu\sigma\rangle \otimes \rho_\Sigma(0)\Big]\,,\end{aligned} \tag{47}$$

where $\rho_\Sigma(0) = \frac{1}{2}|\Uparrow\rangle\langle\Uparrow| + \frac{1}{2}|\Downarrow\rangle\langle\Downarrow|$ is the spin unpolarized density matrix in the space of non-itinerant magnetic moment. If the impurity is spin polarized, e.g., by an external magnetic field aligned along the spin quantization axis, then one uses

$$\rho_\Sigma(B) = \frac{1}{1+\mathrm{e}^{-\beta(g\mu_\mathrm{B}B)}}\,|\Uparrow\rangle\langle\Uparrow| + \frac{1}{1+\mathrm{e}^{\beta(g\mu_\mathrm{B}B)}}\,|\Downarrow\rangle\langle\Downarrow|\,, \tag{48}$$

where g is the g-factor of the local magnetic moment, μ_B stands for the Bohr magneton and $\beta = (k_\mathrm{B}T)^{-1}$. In what follows we consider only the unpolarized ($B=0$) case and in the result we get

$$\begin{aligned}\left|\langle \mathbf{k}'\nu'\sigma' \,|\, \mathrm{T}(E) \,|\, \mathbf{k}\nu\sigma\rangle\right|^2 = \frac{1}{2}\,\frac{1}{(2N)^2}\,\Big\{|\delta_{\sigma\sigma'}\left|\mathrm{T}_1(E)\right|^2 \\ + \tfrac{1}{4}\left|\mathrm{T}_1(E) + (\sigma\cdot\sigma')\,\mathrm{T}_0(E)\right|^2\Big\}\,,\end{aligned} \tag{49}$$

where $E=\varepsilon_{\mathbf{k}\nu\sigma}$ is given by Eq. (6), $\mathrm{T}_\ell(E)$ is specified by Eq. (43), factor $\frac{1}{2}$ comes from averaging over the unpolarized impurity magnetic moment and

the sign factor $\sigma \cdot \sigma' = \pm 1$ for the parallel/antiparallel spin orientations. Considering the transition rate for a particular scattering process

$$W_{\mathbf{k}\sigma|\mathbf{k}'\sigma'} = \frac{2\pi}{\hbar} \big| \langle \mathbf{k}'\nu'\sigma' \,|\, \mathrm{T}(\varepsilon_{\mathbf{k}\nu\sigma}) \,|\, \mathbf{k}\nu\sigma \rangle \big|^2 \delta\big(\varepsilon_{\mathbf{k}\nu\sigma} - \varepsilon_{\mathbf{k}'\nu'\sigma'}\big) \,. \tag{50}$$

and integrating it over all final states we get spin conserving $1/\tau_{\uparrow\uparrow}(E)$ and spin flip $1/\tau_{\downarrow\uparrow}(E)$ relaxation rates for the given Fermi energy,

$$\frac{1}{\tau_{\sigma\sigma'}(E)} = \frac{1}{\tau_{\sigma'\sigma}(E)} = \frac{2\pi}{\hbar} \frac{\eta_{\mathrm{imp}}}{2} \Big\{ \delta_{\sigma\sigma'} \big|\mathrm{T}_1(E)\big|^2 + \tfrac{1}{4} \big|\mathrm{T}_1(E) + (\sigma\cdot\sigma')\,\mathrm{T}_0(E)\big|^2 \Big\} \frac{|E|}{W^2} \,. \tag{51}$$

Spin lifetime $\tau_{\mathrm{s}}(E)$ for the given Fermi energy E at zero temperature is defined via $1/\tau_{\mathrm{s}}(E) = 1/\tau_{\downarrow\uparrow}(E) + 1/\tau_{\uparrow\downarrow}(E)$ and equals

$$\frac{1}{\tau_{\mathrm{s}}(E)} = \frac{2\pi}{\hbar}\, \eta_{\mathrm{imp}} \big| \tfrac{1}{2}\mathrm{T}_1(E) - \tfrac{1}{2}\,\mathrm{T}_0(E)\big|^2 \frac{|E|}{W^2} \,. \tag{52}$$

Similarly, we define the *momentum lifetime* $\tau_{\mathrm{m}}(E)$, i.e. $1/\tau_{\mathrm{m}} = 1/\tau_{\uparrow\uparrow}(E) + 1/\tau_{\uparrow\downarrow}(E)$,

$$\frac{1}{\tau_{\mathrm{m}}(E)} = \frac{\pi\eta_{\mathrm{imp}}}{\hbar} \Big\{ \tfrac{3}{2} \big|\mathrm{T}_1(E)\big|^2 + \tfrac{1}{2} \big|\mathrm{T}_0(E)\big|^2 \Big\} \frac{|E|}{W^2} \,. \tag{53}$$

The left panel in Fig. 8 shows the spin and momentum relaxation rates, i.e., inverses of $\tau_s(E)$ and $\tau_{\mathrm{m}}(E)$, as functions of the Fermi energy (lower scale) and the charge carriers density (upper scale). We again see the clear formation of the resonances which are governed by the denominators of $\mathrm{T}_1(E)$ and $\mathrm{T}_0(E)$ that enters Eqs. (52) and (53). The resonance peak lying lower in the energy corresponds to the singlet state ($\ell = 0$). The higher peak comes from the triplet ($\ell = 1$). Spin relaxation gets strongly enhanced in the resonances; away it falls to the values typical for a perturbative regime.

Similarly as in the previous chapter we can look for DOS in the presence of a magnetic impurity. The derivation is fully analogical to the above case and the result is as follows

$$\mathcal{V}(E) = 8N \frac{|E|}{W^2} \Theta\big[W - |E|\big] + \frac{1}{\pi}\, \mathrm{Im} \sum_{\ell} \big[\tfrac{d}{dE} G_{00}(E)\big]\, (2\ell+1)\, \mathrm{T}_\ell(E) \,. \tag{54}$$

The right panel in Fig. 8 compares the perturbed DOS per atom and spin $\frac{1}{8N}\mathcal{V}(E)$ (solid line) with the same for the pristine graphene. We observe clear formations of two resonance peaks. The singlet resonance emerges below the graphene neutrality point at $E_{\mathrm{r},\ell=0} \simeq -69.4\,\mathrm{meV}$ and possesses

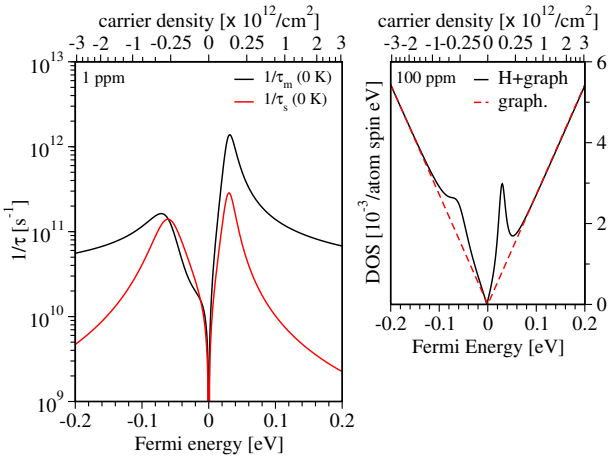

Fig. 8. Left: Momentum relaxation $1/\tau_{\rm m}$ (black line) and spin relaxation $1/\tau_{\rm s}$ (red line) rates at zero temperature as functions of the Fermi level (lower scale) and charge carriers density (upper scale) for the hydrogen concentration $\eta_{\rm imp} = 1\,$ppm. Orbital parameters $\varepsilon = 0.16\,$eV, $\omega = 7.5\,$eV and the exchange coupling $J = -0.4\,$eV. The relaxation enhances near the resonance energies. Without the magnetic exchange there is only one narrow orbital resonance at $E_{\rm r} \simeq 7.4\,$meV. The exchange coupling splits it into the singlet resonance $E_{{\rm r},\ell=0} \simeq -69.4\,$meV and the triplet resonance $E_{{\rm r},\ell=1} \simeq 32.5\,$meV, respectively. Right: Density of states per carbon and spin for hydrogenated graphene (solid line) with exchange coupling and unperturbed graphene (dashed line). To amplify the resolution we used impurity concentration $\eta_{\rm imp} = 100\,$ppm.

a relatively wide width $\Gamma_{\ell=0} \simeq 63.6\,$meV. In contrast, the triplet resonance occurs above the charge neutrality at $E_{{\rm r},\ell=1} \simeq 32.5\,$meV and is more narrower with $\Gamma_{\ell=1} \simeq 24\,$meV.

We see that the resonant enhancement of spin relaxation requires two ingredients—resonant impurity scatterer that simultaneously possesses a magnetic moment. Then, there are two associated time scales in the system which could cooperate. The width of the resonance Γ defines a time scale $\tau_{\rm dwell} = \hbar/\Gamma$ for an electron dwelling within the impurity region. The exchange coupling on the other side splits the singlet and triplet states by $4J$, so it effectively acts as an "exchange magnetic field" producing Zeeman splitting. Hence the Larmor time of precession in such an "exchange magnetic field" equals $\tau_{\rm Larm} = \hbar/|2J|$. Qualitatively, if the electron with the incident energy close to the resonance energy enters the system and becomes trapped by the impurity, then it will spend time $\tau_{\rm dwell}$ orbiting around. During this it experiences magnetic exchange and the composite spin state

of "electron+magnetic moment" evolves in the "effective exchange field". If $\tau_{\rm Larm} \lesssim \tau_{\rm dwell}$ ($|2J| \gtrsim \Gamma$), then there is enough time for the exchange magnetic field to mix the incoming spin, such that the electron leaving the impurity region will have a completely randomized spin orientation, see Fig. 9. For hydrogen we have $|2J|$ of orders of hundreds of meV and Γ of orders of tens meV, so we are in the resonance enhancement regime.

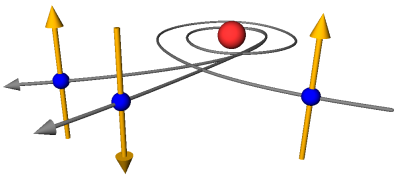

Fig. 9. Resonant scatterer with exchange coupling would relax simultaneously momentum and spin of the incident electrons assuming the exchange strength $|2J|$ is greater then the resonance width Γ.

To account for temperature effects and non-uniformities of the Fermi level within the sample due to charged impurities we should employ to $1/\tau_s(E)$ thermal broadening and broadening due to electron-hole puddles. They are shortly explained in the forthcoming section.

5. Spin relaxation–thermal broadening and charge puddles.

The spin relaxation rate is obtained by formulating rate equations. Suppose we have an electron spin accumulation in graphene described by the spin-dependent chemical potential μ_σ. The electron distribution functions differ from equilibrium as $f_{k\sigma} = f^0_k + \delta f_{k\sigma}$, where

$$\delta f_{k\sigma} \approx \left(-\frac{\partial f^0_k}{\partial \varepsilon_k}\right)\Bigg|_{\varepsilon_F} (\mu_\sigma - \varepsilon_F). \tag{55}$$

We denoted as $f^0_k = f^0(\varepsilon_k)$ the Fermi-Dirac function at temperature T, ε_k the electron one-particle energy, and ε_F the Fermi level. The electron spin accumulation s equals

$$s = \sum_k f_{k\uparrow} - f_{k\downarrow} = \sum_k \left(-\frac{\partial f^0_k}{\partial \varepsilon_k}\right)\Bigg|_{\varepsilon_F} \mu_s, \tag{56}$$

with $\mu_s = \mu_\uparrow - \mu_\downarrow$. The spin relaxation rate is defined from the equation,

$$\frac{\partial s}{\partial t} = \sum_k \left(-\frac{\partial f_k^0}{\partial \varepsilon_k}\right)\Big|_{\varepsilon_F} \frac{\partial \mu_s}{\partial t} \equiv -\frac{s}{\tau_{\rm s}(\varepsilon_F)}. \tag{57}$$

Let $W_{k\uparrow\Downarrow|k'\downarrow\Uparrow}$ be the spin flip rate for the transition of an electron with momentum k and spin up ($\uparrow$), in the presence of an impurity with spin down ($\Downarrow$), to another state of momentum k' and spin down ($\downarrow$), and impurity spin up ($\Uparrow$). Similarly for $W_{k\uparrow\Uparrow|k'\uparrow\Uparrow}$ and $W_{k\uparrow\Downarrow|k'\uparrow\Downarrow}$ etc. In our particular case $k = (\mathbf{k}\nu)$ and $k' = (\mathbf{k}'\nu')$. For example, from Eq. (46) we get

$$W_{k\uparrow\Downarrow|k'\downarrow\Uparrow} = \frac{2\pi}{\hbar}\,\frac{1}{(2N)^2}\left|\frac{\mathrm{T}_1(E) - \mathrm{T}_0(E)}{2}\right|^2 \delta(\varepsilon_{k\uparrow\Downarrow} - \varepsilon_{k'\downarrow\Uparrow}) \tag{58}$$

and similarly for other rates. Let the probability of the impurity spin being $\Sigma = \{\Uparrow, \Downarrow\}$ be P_Σ. The rate equation for the spin up electron with momentum k is

$$\begin{aligned}
\frac{\partial f_{k\uparrow}}{\partial t} = {} & \\
& \sum_{k'}\Big\{W_{k'\downarrow\Uparrow|k\uparrow\Downarrow}\; P_\Uparrow f_{k'\downarrow}\,(1 - f_{k\uparrow}) - W_{k\uparrow\Downarrow|k'\downarrow\Uparrow}\; P_\Downarrow f_{k\uparrow}\,(1 - f_{k'\downarrow})\Big\} + \\
& + \sum_{k'}\Big\{W_{k'\uparrow\Uparrow|k\uparrow\Uparrow}\; P_\Uparrow f_{k'\uparrow}\,(1 - f_{k\uparrow}) - W_{k\uparrow\Uparrow|k'\uparrow\Uparrow}\; P_\Uparrow f_{k\uparrow}\,(1 - f_{k'\uparrow})\Big\} + \\
& + \sum_{k'}\Big\{W_{k'\uparrow\Downarrow|k\uparrow\Downarrow}\; P_\Downarrow f_{k'\uparrow}\,(1 - f_{k\uparrow}) - W_{k\uparrow\Downarrow|k'\uparrow\Downarrow}\; P_\Downarrow f_{k\uparrow}\,(1 - f_{k'\uparrow})\Big\}.
\end{aligned} \tag{59}$$

The only terms contributing to spin relaxation are spin-flip terms grouped in the first line. The remaining lines are not important for the spin relaxation since they will cancel out. Assuming unpolarized magnetic moments, $P_\Uparrow = P_\Downarrow = 1/2$, and using the symmetries of the spin-flip rates, we get

$$\begin{aligned}
\frac{\partial f_{k\uparrow}}{\partial t} = {} & -\tfrac{1}{2}\sum_{k'} W_{k\uparrow\Downarrow|k'\downarrow\Uparrow}\,(f_{k\uparrow} - f_{k'\downarrow}) + \\
& - \tfrac{1}{2}\sum_{k'}\big(W_{k\uparrow\Uparrow|k'\uparrow\Uparrow} + W_{k\uparrow\Downarrow|k'\uparrow\Downarrow}\big)\,(f_{k\uparrow} - f_{k'\uparrow})
\end{aligned} \tag{60}$$

and similarly for the rate of $f_{k\downarrow}$. We can then write

$$\frac{\partial s}{\partial t} = \sum_k \frac{\partial f_{k\uparrow}}{\partial t} - \frac{\partial f_{k\downarrow}}{\partial t} = -\sum_k\sum_{k'} W_{k\uparrow\Downarrow|k'\downarrow\Uparrow}\,(\delta f_{k\uparrow} - \delta f_{k'\downarrow}) = -\frac{s}{\tau_{\rm s}}. \tag{61}$$

Substituting the spin accumulation and comparing with the defining equation for $\tau_{\rm s}$ we get

$$\frac{1}{\tau_{\rm s}(\varepsilon_F, T)} = \frac{\sum_k \sum_{k'} \left(-\partial f_k^0/\partial\varepsilon_k\right) W_{k\uparrow\Downarrow|k'\downarrow\Uparrow}}{\sum_k \left(-\partial f_k^0/\partial\varepsilon_k\right)}\,, \tag{62}$$

where the temperature T and the Fermi level ε_F are the parameters of the equilibrium Fermi-Dirac distribution f_k^0. This equation should be used when evaluating the temperature dependence of spin relaxation rates.

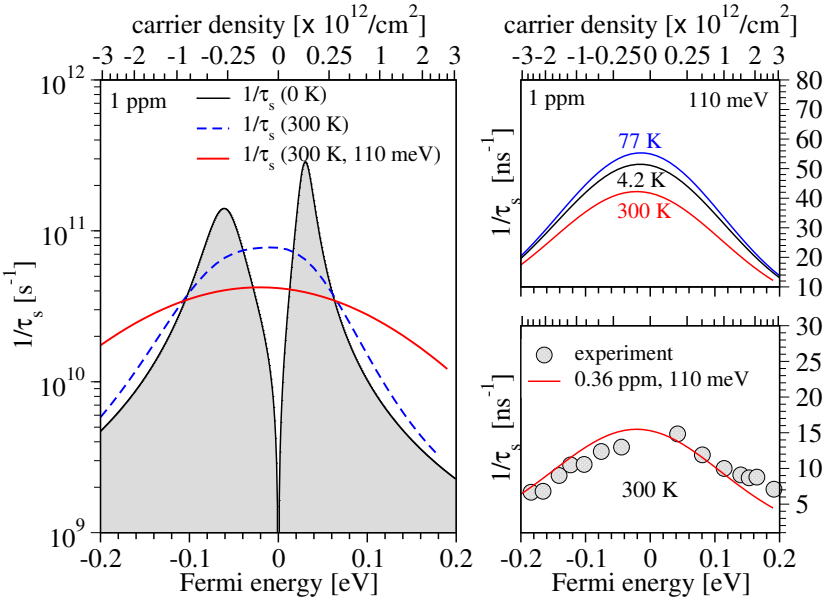

Fig. 10. Resonant enhancement of spin relaxation in graphene. Exchange coupling $J = -0.4$ eV and impurity fraction $\eta_{\rm imp}$ in ppm is indicated. Left panel: Spin relaxation rate $1/\tau_s$ as a function of energy/carrier density, at 0 K, at 300 K, and at 300 K broadened by puddles with energy fluctuations of 110 meV. Top-right panel: Broadened $1/\tau_s$ at different temperatures. Bottom-right panel: Comparison between theory and experiment (graphene data from Ref. 47) at 300 K. The figure is adopted from Ref. 23.

In reality the electron-hole puddles and other charge impurities would affect the Fermi level which will not be uniform within the sample, see Refs. 48,49. Typically the Fermi level oscillates about $\pm\sigma_b$, where σ_b equals 75 - 110 meV. This would correspond to the charge carriers density variation of about $\pm\,(5\text{-}10)\times10^{11}/\mathrm{cm}^2$. The simplest phenomenological way how to include all the broadening effects would be the convolution of $1/\tau_{\rm s}(\varepsilon_F, T)$ with the Gaussian kernel with the standard deviation σ_b,

$$\frac{1}{\tau_{\rm s}(\varepsilon_F, T, \sigma_{\rm br})} = \frac{1}{2\sqrt{\pi}\sigma_b} \int\limits_{-\infty}^{\infty} {\rm d}E\, \frac{1}{\tau_{\rm s}(E,T)}\, \exp\left(-\frac{(E-\varepsilon_F)^2}{2\sigma_b^2}\right). \qquad (63)$$

The results for hydrogenated graphene for different temperatures and the fixed value of broadening $\sigma_{\rm b} = 110$ meV are plotted in Fig. 10. Zero temperature rates at the left panel of Fig. 10 with the singlet and triplet split resonance peaks merge due to thermal and electron-hole puddles broadening effects. From the top-right panel in Fig. 10 we can conclude that the temperature dependence of $1/\tau_s$ is rather weak, essentially given by Fermi broadening of the resonance structure. Finally, in the bottom-right panel of Fig. 10 we compare the calculated spin relaxation rates with experiment, with the adjusted value of $\eta_{\rm imp} = 0.36\,$ppm. The agreement is remarkable. In fact, one can find a nice agreement for a large window of J by adjusting $\sigma_{\rm b}$ and $\eta_{\rm imp}$. Vacancies and different adatoms are well covered by this mechanism.

Acknowledgements

We acknowledge supported from DFG SFB 689 and the EU Seventh Framework Programme under Grant Agreement No. 604391 Graphene Flagship.

References

1. A. K. Geim and K. S. Novoselov, The rise of graphene, *Nat. Materials* **6**, 183 (2007).
2. A. H. Castro Neto, Another spin on graphene, *Science* **332**, 315 (2011).
3. I. Žutić, J. Fabian and S. Das Sarma, Spintronics: Fundamentals and applications, *Rev. Mod. Phys.* **76**, p. 323 (2004).
4. J. Fabian, A. Matos-Abiague, C. Ertler, P. Stano and I. Žutić, Semiconductor spintronics, *Acta Phys. Slovaca* **57**, 565 (2007).
5. W. Han, R. K. Kawakami, M. Gmitra and J. Fabian, Graphene spintronics, *Nat. Nano.* **9**, p. 794 (2014).
6. N. Tombros, C. Józsa, M. Popinciuc, H. T. Jonkman and B. J. van Wees, Electronic spin transport and spin precession in single graphene layers at room temperature, *Nature* **448**, p. 571 (2007).
7. N. Tombros, S. Tanabe, A. Veligura, C. Jozsa, M. Popinciuc, H. T. Jonkman and B. J. van Wees, Anisotropic spin relaxation in graphene, *Phys. Rev. Lett.* **101**, p. 046601 (2008).
8. K. Pi, W. Han, K. M. McCreary, A. G. Swartz, Y. Li and R. K. Kawakami, Manipulation of spin transport in graphene by surface chemical doping, *Phys. Rev. Lett.* **104**, p. 187201 (2010).
9. T.-Y. Yang, J. Balakrishnan, F. Volmer, A. Avsar, M. Jaiswal, J. Samm, S. R. Ali, A. Pachoud, M. Zeng, M. Popinciuc,

G. Güntherodt, B. Beschoten and B. Özyilmaz, Observation of long spin-relaxation times in bilayer graphene at room temperature, *Phys. Rev. Lett.* **107**, p. 047206 (2011).
10. W. Han and R. K. Kawakami, Spin relaxation in single-layer and bilayer graphene, *Phys. Rev. Lett.* **107**, p. 047207 (2011).
11. A. Avsar, T.-Y. Yang, S. Bae, J. Balakrishnan, F. Volmer, M. Jaiswal, Z. Yi, S. R. Ali, G. Güntherodt, B. H. Hong, B. Beschoten and B. Özyilmaz, Toward wafer scale fabrication of graphene based spin valve devices, *Nano Letters* **11**, 2363 (2011).
12. S. Jo, D.-K. Ki, D. Jeong, H.-J. Lee and S. Kettemann, Spin relaxation properties in graphene due to its linear dispersion, *Phys. Rev. B* **84**, p. 075453 (2011).
13. R. G. Mani, J. Hankinson, C. Berger and W. A. de Heer, Observation of resistively detected hole spin resonance and zero-field pseudo-spin splitting in epitaxial graphene, *Nature Commun.* **3**, p. 996 (2012).
14. D. Huertas-Hernando, F. Guinea and A. Brataas, Spin-orbit coupling in curved graphene, fullerenes, nanotubes, and nanotube caps, *Phys. Rev. B* **74**, p. 155426 (2006).
15. B. Dora, F. Muranyi and F. Simon, Electron spin dynamics and electron spin resonance in graphene, *Eur. Phys. Lett.* **92**, p. 17002 (2010).
16. J.-S. Jeong, J. Shin and H.-W. Lee, Curvature-induced spin-orbit coupling and spin relaxation in a chemically clean single-layer graphene, *Phys. Rev. B* **84**, p. 195457 (2011).
17. V. K. Dugaev, E. Y. Sherman and J. Barnaś, Spin dephasing and pumping in graphene due to random spin-orbit interaction, *Phys. Rev. B* **83**, p. 085306 (2011).
18. C. Ertler, S. Konschuh, M. Gmitra and J. Fabian, Electron spin relaxation in graphene: The role of the substrate, *Phys. Rev. B* **80**, p. 041405 (2009).
19. P. Zhang and M. W. Wu, Electron spin diffusion and transport in graphene, *Phys. Rev. B* **84**, p. 045304 (2011).
20. H. Ochoa, A. H. Castro Neto and F. Guinea, Elliot-Yafet mechanism in graphene, *Phys. Rev. Lett.* **108**, p. 206808 (2012).
21. D. V. Fedorov, M. Gradhand, S. Ostanin, I. V. Maznichenko, A. Ernst, J. Fabian and I. Mertig, Impact of electron-impurity scattering on the spin relaxation time in graphene: A first-principles study, *Phys. Rev. Lett.* **110**, p. 156602 (2013).
22. D. V. Tuan, F. Ortmann, D. Soriano, S. O. Valenzuela and S. Roche, Pseudospin-driven spin relaxation mechanism in graphene, *Nat. Phys.*

10, p. 857 (2014).
23. D. Kochan, M. Gmitra and J. Fabian, Spin relaxation mechanism in graphene: Resonant scattering by magnetic impurities, *Phys. Rev. Lett.* **112**, p. 116602 (2014).
24. M. B. Lundeberg, R. Yang, J. Renard and J. A. Folk, Defect-mediated spin relaxation and dephasing in graphene, *Phys. Rev. Lett.* **110**, p. 156601 (2013).
25. M. M. Ugeda, I. Brihuega, F. Guinea and J. M. Gomez-Rodriguez, Missing atom as a source of carbon magnetism, *Phys. Rev. Lett.* **104**, p. 096804 (2010).
26. R. R. Nair, M. Sepioni, I. L. Tsai, O. Lehtinen, J. Keinonen, A. V. Krasheninnikov, T. Thomson, A. K. Geim and I. V. Grigorieva, Spin-half paramagnetism in graphene induced by point defects, *Nature Physics* **8**, p. 199 (2012).
27. K. M. McCreary, A. G. Swartz, W. Han, J. Fabian and R. K. Kawakami, Magnetic moment formation in graphene detected by scattering of pure spin currents, *Phys. Rev. Lett.* **109**, p. 186604 (2012).
28. O. Yazyev, Emergence of magnetism in graphene materials and nanostructures, *Rep. Prog. Phys.* **73**, p. 056501 (2010).
29. J. Fabian and S. Das Sarma, Spin relaxation of conduction electrons in polyvalent metals: Theory and a realistic calculation, *Phys. Rev. Lett.* **81**, 5624 (Dec 1998).
30. T. O. Wehling, S. Yuan, A. I. Lichtenstein, A. K. Geim and M. I. Katsnelson, Resonant scattering by realistic impurities in graphene, *Phys. Rev. Lett.* **105**, p. 056802 (2010).
31. M. Gmitra, D. Kochan and J. Fabian, Spin-orbit coupling in hydrogenated graphene, *Phys. Rev. Lett.* **110**, p. 246602 (2013).
32. M. H. D. Guimarães, P. J. Zomer, J. Ingla-Aynés, J. C. Brant, N. Tombros and B. J. van Wees, Controlling spin relaxation in hexagonal BN-encapsulated graphene with a transverse electric field, *Phys. Rev. Lett.* **113**, p. 086602 (2014).
33. M. Drögeler, F. Volmer, M. Wolter, B. Terrés, K. Watanabe, T. Taniguchi, G. Güntherodt, C. Stampfer and B. Beschoten, Nanosecond spin lifetimes in single- and few-layer graphene-hBN heterostructures at room temperature, *Nano Letters* **14**, p. 6050 (2014).
34. M. Gmitra, S. Konschuh, C. Ertler, C. Ambrosch-Draxl and J. Fabian, Band-structure topologies of graphene: Spin-orbit coupling effects from first principles, *Phys. Rev. B* **80**, p. 235431 (2009).
35. P. R. Wallace, The band theory of graphite, *Phys. Rev.* **71**, p. 622

(1947).
36. C. A. Coulson and R. Taylor, Studies in graphite and related compounds i: Electronic band structure in graphite: Electronic band structure in graphite, *Proc. Phys. Soc. A* **65**, 815 (1952).
37. W. M. Lomer, The valence bands in two-dimensional graphite, *Proc. Roy. Soc. (London)* **A227**, 330 (1955).
38. J. W. McClure, Band structure of graphite and de Haas-van Alphen effect, *Phys. Rev.* **108**, 612 (1957).
39. J. C. Slonczewski and P. R. Weiss, Band structure of graphite, *Phys. Rev.* **109**, 272 (1958).
40. J. W. McClure and Y. Yafet, Theory of the g-factor of the current carriers in graphite single crystals, in *Proceedings of the Fifth Conference on Carbon*, (Pergamon, New York, 1962).
41. S. Konschuh, M. Gmitra and J. Fabian, Tight binding theory of spin-orbit coupling in graphene, *Phys. Rev. B* **82**, p. 245412 (2010).
42. S. Irmer, T. Frank, S. Putz, M. Gmitra, D. Kochan, and J. Fabian, Spin-orbit coupling in fluorinated graphene, arXiv 1411.0016.
43. J. Callaway, Theory of scattering in solids, *Journal of Mathematical Physics* **5** (1964).
44. S.-Z. Liang and J. Sofo, Impurity state and variable range hopping conduction in graphene, *Phys. Rev. Lett.* **109**, p. 256601 (2012).
45. J. Martin, N. Akerman, G. Ulbricht, T. Lohmann, J. H. Smet, K. von Klitzing and A. Yacoby, Observation of electron-hole puddles in graphene using a scanning single-electron transistor, *Nat Phys* **4**, p. 144 (2008).
46. O. V. Yazyev and L. Helm, Defect-induced magnetism in graphene, *Phys. Rev. B* **75**, p. 125408 (2007).
47. M. Wojtaszek, I. J. Vera-Marun, T. Maassen and B. J. van Wees, Enhancement of spin relaxation time in hydrogenated graphene spin-valve devices, *Phys. Rev. B* **87**, p. 081402 (2013).
48. E. H. Hwang, S. Adam and S. Das Sarma, Carrier transport in two-dimensional graphene layers, *Phys. Rev. Lett.* **98**, p. 186806 (2007).
49. A. Deshpande, W. Bao, F. Miao, C. N. Lau and B. J. LeRoy, Spatially resolved spectroscopy of monolayer graphene on SiO_2, *Phys. Rev. B* **79**, p. 205411 (2009).